# Analysis of Variable Porosity, Thermal Dispersion, and Local Thermal Nonequilibrium on Free Surface Flows Through Porous Media

**Bader Alazmi**

Department of Mechanical Engineering,
Kuwait University,
P.O. Box 5969,
Safat 13060 Kuwait

**Kambiz Vafai**

e-mail: vafai@engr.ucr.edu
University of California, Riverside,
Department of Mechanical Engineering,
A363 Bourns Hall,
Riverside, CA 92521-0425

*Characteristics of momentum and energy transport for free surface flows through porous media are explored in this study. Effects of variable porosity and an impermeable boundary on the free surface front are analyzed. In addition, effects of thermal dispersion and local thermal nonequilibrium (LTNE) are also analyzed. Pertinent parameters such as porosity, Darcy number, inertia parameter, Reynolds number, particle diameter, and solid-to-fluid conductivity ratio are used to investigate the significance of the above mentioned effects. Results show that considering the effect of variable porosity is significant only in the neighborhood of the solid boundary. The range of parameters which enhance the dispersion and LTNE effects are prescribed. Finally, it is shown that adding the effect of thermal dispersion to LTNE increases the sensitivity of LTNE between the two phases.*
[DOI: 10.1115/1.1723470]

*Keywords: Convection, Heat Transfer, Porous Media*

## 1 Introduction

Incompressible free surface fluid flow in porous media has been the subject of many studies in the last few decades because of its importance in many applications such as geophysics, die filling, metal processing, agricultural and industrial water distribution, oil recovery techniques, and injection molding. One of the earliest studies in this field was performed by Muskat [1] who considered a one-dimensional Darcy's flow model to analyze the linear encroachment of two fluids in a narrow channel. Recently, an analytical solution for linear encroachment in two immiscible fluids in a porous medium was presented in Srinivasan and Vafai [2]. They obtained a closed form solution, for the temporal free surface fluid front, that accounts for boundary and inertia effects. Their results show that for higher permeabilities Muskat's model underestimates the total time needed for the encroaching fluid to reach the end of the channel. Furthermore, they show that implementing their analytical solution is essential for cases of low mobility ratios.

Later on, Chen and Vafai [3] investigated the free surface transport through porous media numerically using the Marker and Cell method. They extended the study of Srinivasan and Vafai [2] to include free surface energy transport in their investigation. Another study performed by Chen and Vafai [4] considered interfacial tension effects on the free surface transport in porous media. Their results show that surface tension can be neglected for high Reynolds number flows.

Additional effects such as variable porosity, thermal dispersion and LTNE have been shown to be quite significant for a number of practical situations and were not studied in the earlier related works [1–4]. Vafai [5,6] and Vafai et al. [7] investigated analytically and experimentally the effect of variable porosity on fluid flow and heat transfer in porous media. It has been shown that the channeling effect can be significant at the neighborhood of solid boundaries. Several other studies considered the effect of thermal dispersion in porous media such as Amiri and Vafai [8], Hwang

et al. [9]. It is found that ignoring the effect of thermal dispersion might lead to inaccurate predictions of heat transfer for some practical applications. The assumption of local thermal equilibrium between the solid and fluid phases is not valid for some engineering applications where temperature discrepancies exist between the phases. LTNE in porous media has been investigated by many researchers such as Lee and Vafai [10], Quintard and Whitaker [11] and Quintard et al. [12]. Quintard and Whitaker [13] analyzed the mass flux boundary condition at a moving fluid-fluid interface. Their analysis suggests a mass jump condition for a singular surface at the moving boundary which depends on the concentration at the interface. Recently, the same authors [14] have considered the problem of dissolution of an immobile phase caused by mass transfer to a second phase which generates a moving free surface between the two phases. In [13,14], a general shape of the free surface front is used in the analysis to derive the volume averaged governing equations and boundary conditions. However, it is practically reasonable to assume a flat free surface at the interface of the two phases. Therefore, the main objective of this study is to investigate the effects of variable porosity, thermal dispersion and LTNE on the free surface fluid flow and heat transfer through porous media.

## 2 Analysis

Geometry and Physical properties are chosen to be similar to those given in previous related studies [2,3] for the purpose of comparison. Description of the system under consideration is shown in Fig. 1. The volume-averaged governing equations are given as [15] follows:

**Continuity Equation.**

$$\nabla \cdot \langle V \rangle = 0 \tag{1}$$

**Momentum Equation.**

$$\frac{\rho_f}{\varepsilon}\langle (V\nabla)V \rangle = -\frac{\mu_f}{K}\langle V \rangle - \frac{\rho_f F \varepsilon}{\sqrt{K}}[\langle V \rangle \langle V \rangle]J + \frac{\mu_f}{\varepsilon}\nabla^2\langle V \rangle - \nabla\langle P \rangle^f \tag{2}$$
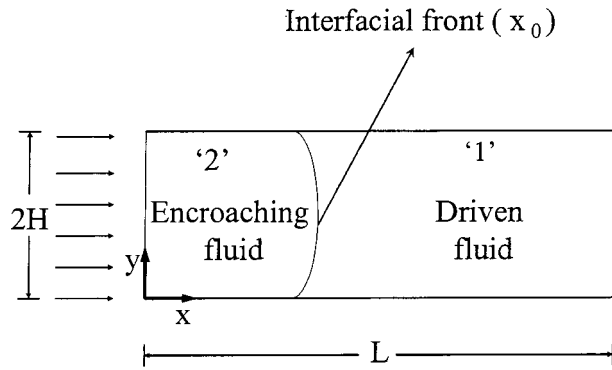
**Fig. 1 Schematic diagram of the free surface front and the corresponding coordinate system**



(a)



(b)

**Fig. 2 Comparison between the present results and the numerical results in Chen and Vafai [3]: (a) temporal free surface distribution using constant Darcy number; and (b) temperature contours for $Re_k=5.72\times10^{-4}$, $Da=1.0\times10^{-6}$ at $t=0.5$ s**



(a)



(b)
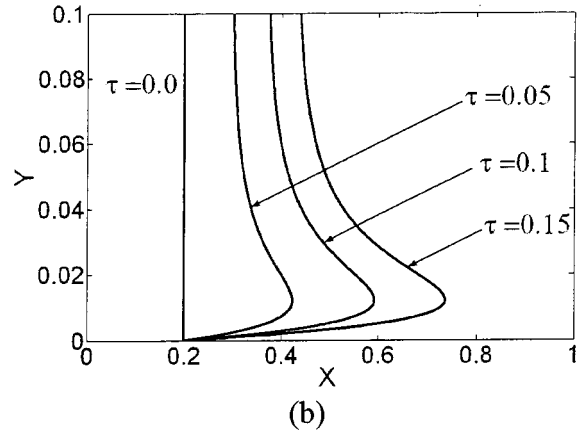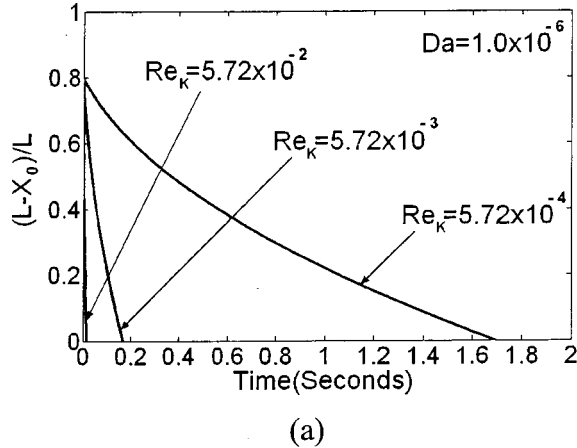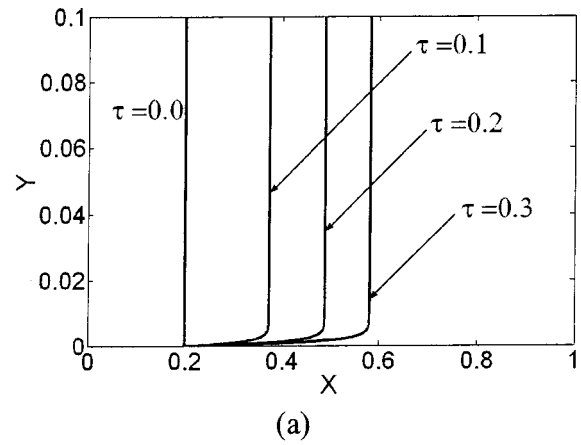
**Fig. 3 Progress of the interfacial front for (a) constant porosity category with $Da=1.0\times10^{-6}$, $\varepsilon=0.8$, $\Lambda=10.0$, and $Re=100$; and (b) variable porosity category with $\varepsilon_\infty=0.45$, $b=0.98$, $c=2.0$, $Re=100$, and $d_P/H=0.05$**

$$a_{sf}=\frac{6(1-\varepsilon)}{d_p} \qquad (6)$$

Effective conductivities of both phases are defined as

$$k_{f\,eff}=\varepsilon k_f \qquad (7)$$

$$k_{s\,eff}=(1-\varepsilon)k_s \qquad (8)$$

When effects of thermal dispersion are present, axial and lateral effective conductivities of the fluid phase can be represented, respectively, as [8]

$$(k_{f\,eff})_x=\left[\varepsilon+0.5\mathrm{Pr}\left(\frac{\rho_f u d_p}{\mu}\right)\right]k_f \qquad (9)$$

$$(k_{f\,eff})_y=\left[\varepsilon+0.1\mathrm{Pr}\left(\frac{\rho_f u d_p}{\mu}\right)\right]k_f \qquad (10)$$

Furthermore, when variation of porosity near the impermeable boundaries is present, porosity, permeability and the geometric function $F$ may be expressed as [5,6]

$$\varepsilon=\varepsilon_\infty\left[1+b\,\exp\left(\frac{-cy}{d_p}\right)\right] \qquad (11)$$

$$K=\frac{\varepsilon^3 d_p^2}{150(1-\varepsilon)} \qquad (12)$$

**Fluid Phase and Solid Phase Energy Equations[8].**

$$\langle\rho_f\rangle^f c_f\langle V\rangle\nabla\langle T_f\rangle^f=\nabla(k_{f\,eff}\nabla\langle T_f\rangle^f)+h_{sf}a_{sf}(\langle T_s\rangle^s-\langle T_f\rangle^f) \qquad (3)$$

$$0=\nabla(k_{s\,eff}\nabla\langle T_s\rangle^s)-h_{sf}a_{sf}(\langle T_s\rangle^s-\langle T_f\rangle^f) \qquad (4)$$

The fluid-to-solid heat transfer coefficient and the specific surface area are expressed as [8]

$$h_{sf}=\frac{k_f}{d_p}\left[2+1.1\mathrm{Pr}^{1/3}\left(\frac{\rho_f u d_p}{\mu_f}\right)^{0.6}\right] \qquad (5)$$
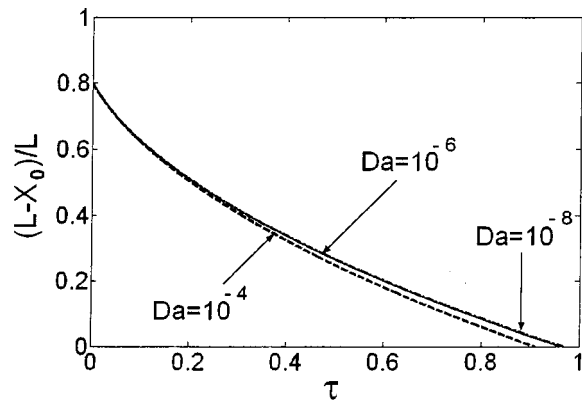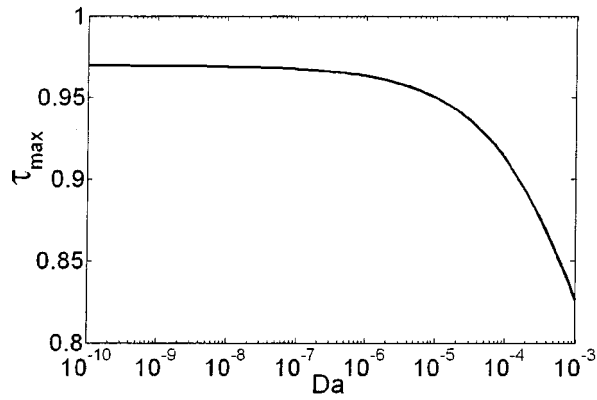
Fig. 4 Effect of Darcy number for the constant porosity category using $\Lambda=10.0$, Re=100 and $\varepsilon=0.8$ on (a) the temporal free surface front; and (b) the total time to reach the channel exit ($\tau_{max}$)



Fig. 5 Effect of Inertia parameter for the constant porosity category using $\varepsilon=0.8$, Da=$1.0\times10^{-6}$ and Re=100: (a) On the temporal free surface front; and (b) On the total time to reach the channel exit ($\tau_{max}$)

$$F=\frac{1.75}{\sqrt{150\varepsilon^3}} \quad (13)$$

Results are presented in terms of the average Nusselt numbers ($\overline{Nu}_f$ and $\overline{Nu}_s$). Local Nusselt numbers for both phases are [8]

$$Nu_f=-\frac{4H}{\langle T_f\rangle_w^f-\langle T_f\rangle_m^f}\left(\frac{\partial\langle T_f\rangle^f}{\partial y}\right)_{y=0} \quad (14)$$

$$Nu_s=-\frac{4H}{\langle T_s\rangle_w^s-\langle T_s\rangle_m^s}\left(\frac{\partial\langle T_s\rangle^s}{\partial y}\right)_{y=0} \quad (15)$$

where $\langle T_f\rangle_m^f$ and $\langle T_s\rangle_m^s$ are the volume averaged mean fluid and solid temperatures, respectively.

As mentioned earlier, boundary and initial conditions are taken exactly similar to previous studies [2,3].

**Initial Condition.**

$$\text{At} \quad t=0, \quad u=v=0, \quad \text{and} \quad T=T_\infty \quad (16)$$

**Boundary Conditions.**

$$\text{At} \quad x=0, \quad p=p_e, \quad v=0, \quad T=T_e \quad (17)$$

$$\text{At} \quad x=x_0, \quad p=p_\infty, \quad \frac{\partial u}{\partial x}=0, \quad -k_{eff}\frac{\partial T}{\partial x}=h(T-T_\infty) \quad (18)$$

$$\text{At} \quad y=0,2H, \quad u=v=0, \quad T=T_w \quad (19)$$

It is possible to compare the present numerical results to the modified analytical solution given in [3]. The modified analytical solution in [3] is presented in terms of the driven fluid physical properties. However, it is more appropriate to express the solution in terms of the encroaching fluid physical properties. Also, in order to compare the numerical results to the analytical results it is assumed that the viscosity of the driven fluid is smaller for this comparison than the viscosity of the encroaching fluid. As such the modified analytical solution is re-written in a simpler form

$$\frac{x_0}{L}=\frac{-\omega+\sqrt{\left[\omega+(1-\omega)\left(\frac{x_i}{L}\right)\right]^2+(1-\omega)\frac{2K_2\Delta p}{\varepsilon\mu_2 L^2}t}}{(1-\omega)} \quad (20)$$

The above equation, Eq. (20), is only a rearranged format of the solution given in [3] and the new mobility ratio ($\omega$) is the inverse of the one defined in [3]. The present mobility ratio, which is assumed to have a very small value, is defined as

$$\omega=\frac{\mu_1}{\mu_2} \quad (21)$$

Based on the appearance of Eq. (20), we also define a dimensionless time ($\tau$) as

$$\tau=\gamma t \quad (22)$$

where
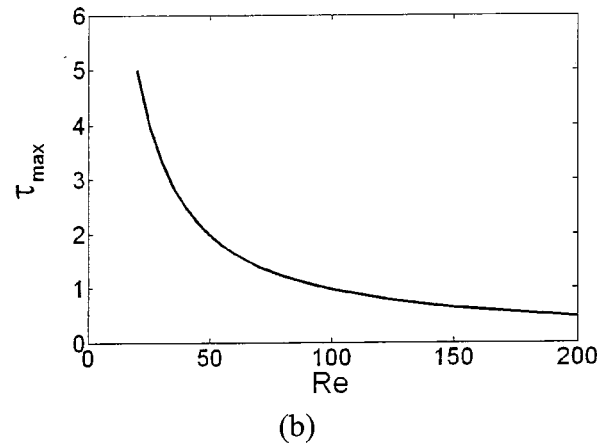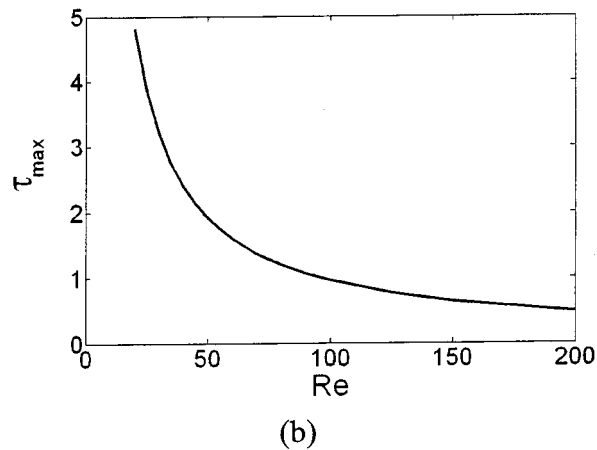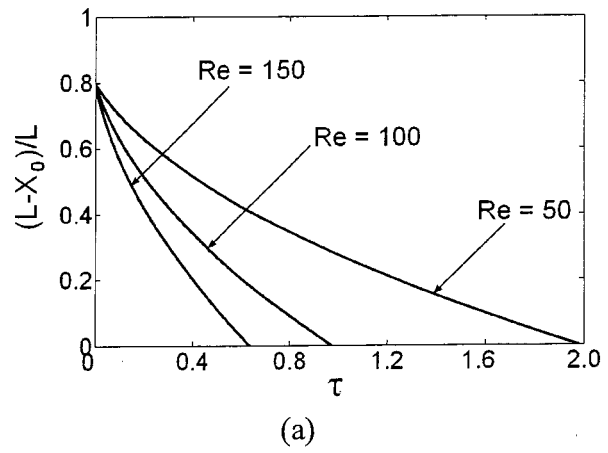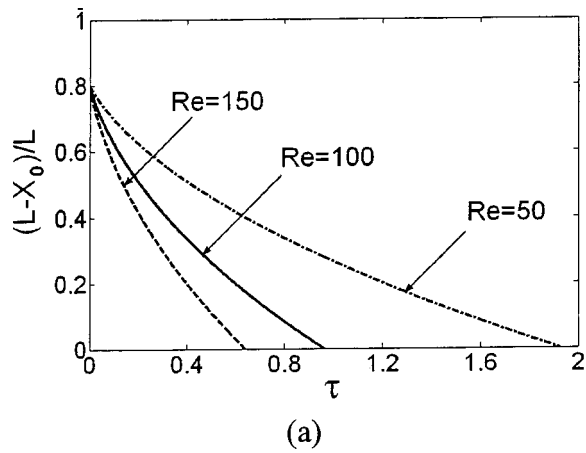
**Fig. 6 Effect of Reynolds number for the constant porosity category using $\varepsilon=0.8$, $Da=1.0\times10^{-6}$ and $\Lambda=10.0$: (a) the temporal free surface front; and (b) the total time to reach the channel exit ($\tau_{max}$)**



**Fig. 7 Effect of Reynolds number for the variable porosity category using $\varepsilon_\infty=0.45$, $b=0.98$, $c=2.0$, and $d_P/H=0.05$ on (a) the temporal free surface front; and (b) the total time to reach the channel exit ($\tau_{max}$)**

$$\gamma=\frac{2K_2\Delta p}{\varepsilon\mu_2L^2} \quad (23)$$

In the above equation, the pressure difference is calculated according to the relation given in Vafai and Kim [16]. Permeability is related to the Darcy number for the constant porosity category while it can be calculated using Eq. (12) for the variable porosity category. Water is considered as the encroaching fluid in the present study.

## 3 Numerical Solution

Variable grids in the $y$-direction and constant grids in the $x$-direction were implemented in the prediction of the flow and temperature fields. Mesh refinements in the vicinity of the free surface front were also applied. This procedure is called interface capturing technique (ICT). It is similar to the one given in Sharif and Wiberg [17]. However, the finite difference method is used in the present study instead of the finite element method used in [17]. ICT eliminates the need for interpolations and extrapolations in the process of predicting the velocity and temperature fields. Since all the nodes coincide with the free surface, the two coupled energy equations are solved using the alternating direction implicit (ADI) method. An iterative solution is required since the two energy equations are coupled.

The requirement that the variation of velocity and temperature distributions is less than $10^{-6}$ between any two consecutive iterations is employed as the criterion for convergence. Numerical ex-

periments were performed to assure grid independent results. A grid size of $201\times501$ was found to provide grid independent results. Due to the presence of symmetry and in order to save a considerable amount of CPU time, numerical computations were performed for the lower half of the physical domain.

In order to verify the accuracy of the present numerical results, comparisons with previous analytical and numerical results are presented in Fig. 2. Figure 2(a) shows comparison between the present numerical results and the modified analytical solution, using a mobility ratio value of zero ($\omega=0$), for the free surface front position. Inputs used to generate Fig. 2(a) were taken to be the same as the ones given in (Fig. 4 of Chen and Vafai [3]). The same is done in Fig. 2(b) which displays the comparison between the current numerical temperature distributions and previous corresponding results in Chen and Vafai [3]. Excellent agreement is found between the present numerical results and results given in Chen and Vafai [3]. Note that the analytical solution given in [2] has been revised by Vafai and Alazmi [18]. They identified some typos in the analytical solution [2] and formulated a modified accurate analytical solution for the problem of linear encroachment in two immiscible fluid systems in a porous medium.

Numerical accuracy for results of velocity, temperature and the average Nusselt number (Nu) was assessed by varying the convergence criteria and the mesh size of the computational domain. Changing the convergence criterion from the utilized value of $10^{-6}$ to $10^{-8}$ always results in a deviation less than 0.5%, 0.2% and 0.1% in velocity, temperature and Nu results respectively. On the other hand, mesh refinements of $401\times1001$ are found to cause

(a)



(b)
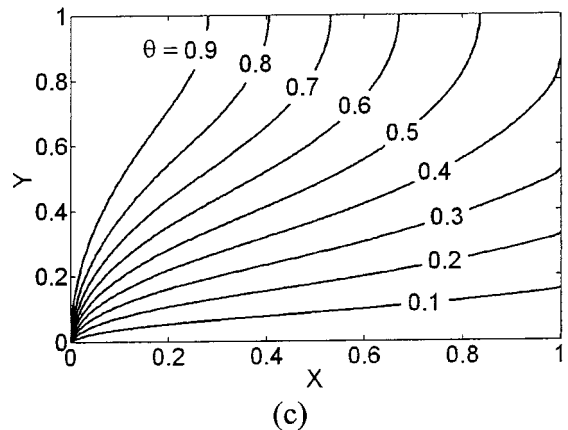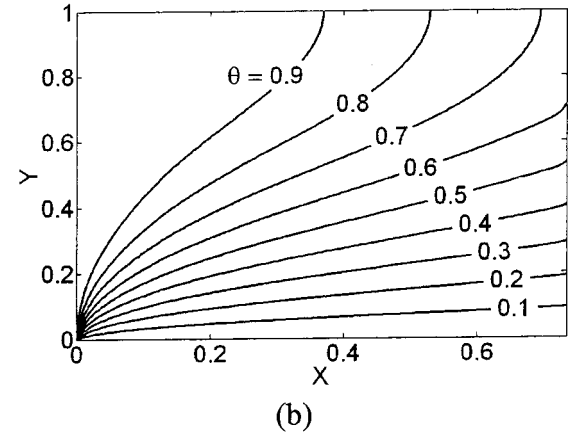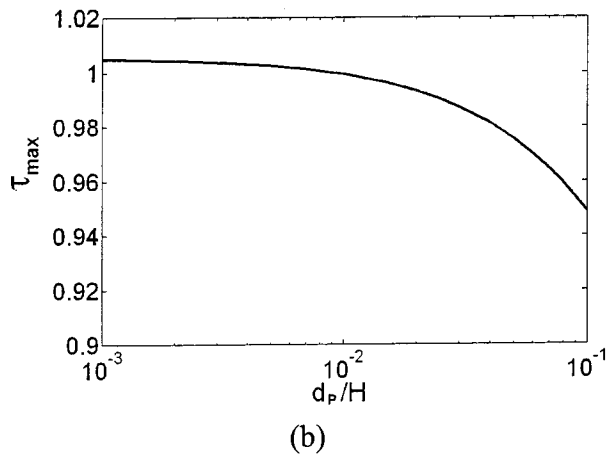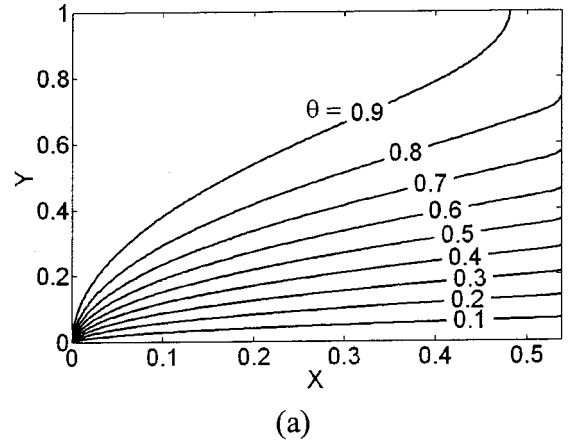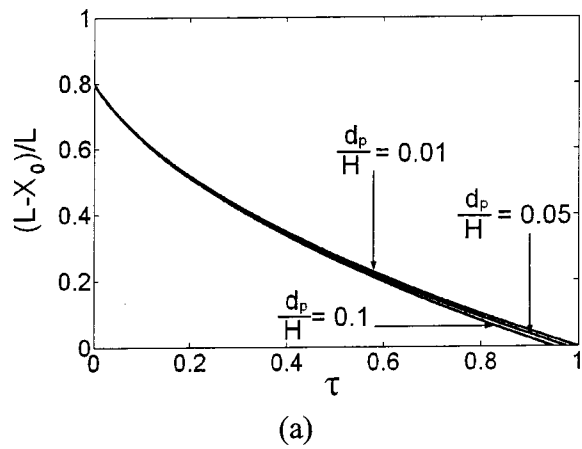
**Fig. 8 Effect of particle diameter for the variable porosity category using $\varepsilon_\infty$=0.45, $b$=0.98, $c$=2.0, and Re=100 on (a) the temporal free surface front; and (b) the total time to reach the channel exit ($\tau_{max}$)**

the results of velocity, temperature and Nu to deviate from those of the utilized mesh size of 201×501 by less than 0.8%, 0.3%, and 0.2%, respectively.

## 4 Results and Discussion

To show the effect of utilizing the constant porosity assumption, results for both constant and variable porosity will be discussed here. Figure 3(a) shows the progress of the interfacial front using constant porosity as a function of time while Fig. 3(b) shows the same using variable porosity. For both cases the flow is assumed to have the same initial position. However, the development of the variable porosity flow is different than the one using constant porosity. It is evident that the effect of variable porosity, which is the case for a number of engineering applications, is more prominent in the neighborhood of the solid boundary. This phenomenon is called the channeling effect which was discussed in detail in [5–6] and will not be discussed here. Our goal here is to analyze the effects of pertinent parameters such as porosity, Darcy number and Reynolds number on the residence time, $\tau_{max}$, for the encroaching fluid under both constant and variable porosity conditions.

**4.1 Constant Porosity.** For the constant porosity category, the reference value of dimensionless time $\tau$ is based on the choice of intermediate values for the pertinent parameters. These reference values are 0.8 for the porosity, $10^{-6}$ for the Darcy number, 100 for the Reynolds number and 10 for the inertia parameter. For a wide range of Darcy number values, $10^{-10}$ to $10^{-6}$ in the



(a)



(b)



(c)

**Fig. 9 Temporal dimensionless temperature profiles including thermal dispersion effects, $\varepsilon$=0.8, Da=$10^{-6}$, Re=100, $\Lambda$=10, $\kappa$=15.0, and $d_P/H$=0.05: (a) $\tau$=0.25, (b) $\tau$=0.5, and (c) $\tau$=$\tau_{max}$**

present study, it is found that the required $\tau_{max}$ to reach the end of the channel is almost the same. However, higher Darcy numbers allow the fluid to reach the end of the channel in a shorter time as shown in Fig. 4. Effect of inertia parameter ($\Lambda$) on the temporal free surface front location is displayed in Fig. 5. It is found that the inertia parameter has less influence on the results when other parameters are fixed. The inertia parameter and $\tau_{max}$ show an inversely linear proportional relation as shown in Fig. 5(b). As expected, Reynolds number has the most significant effect on the progress of the free surface front. Its effect is shown in Fig. 6 where higher Reynolds numbers require significantly shorter time for the fluid to reach the end of the channel.
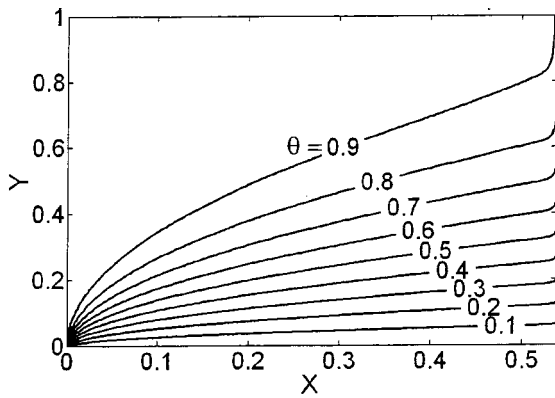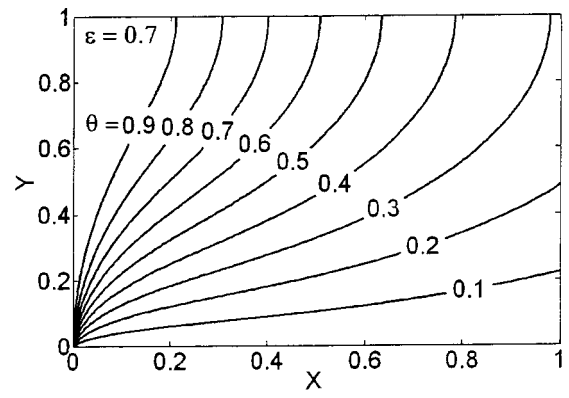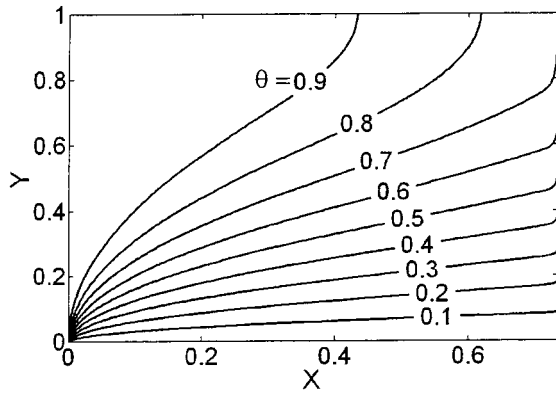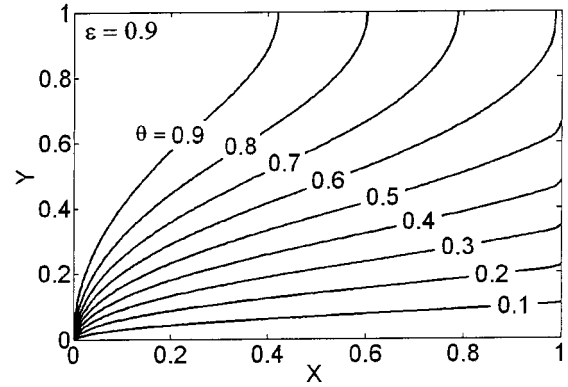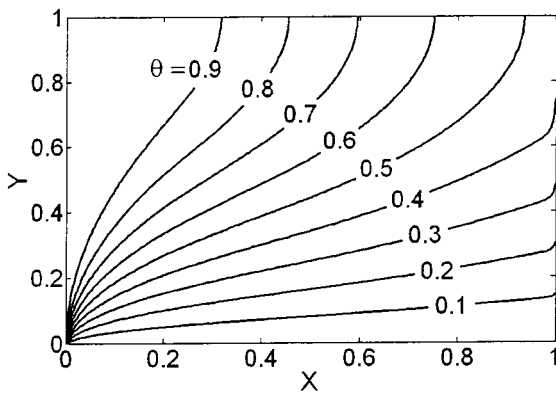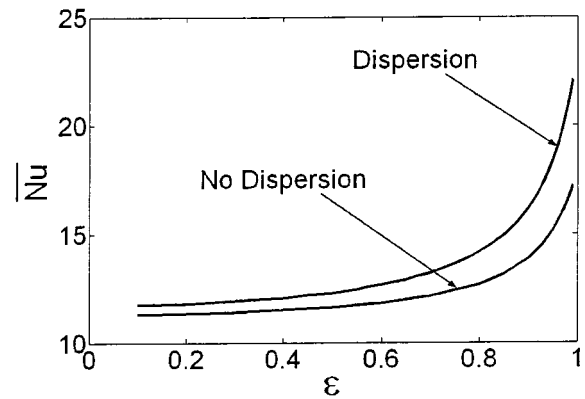
Fig. 10 Temporal dimensionless temperature profiles excluding thermal dispersion effects, $\varepsilon=0.8$, $Da=10^{-6}$, $Re=100$, $\Lambda=10$, $\kappa=15.0$, and $d_P/H=0.05$: (a) $\tau=0.25$, (b) $\tau=0.5$, and (c) $\tau=\tau_{max}$



Fig. 11 Effect of porosity for the thermal dispersion category using $Da=10^{-6}$, $Re=100$, $\Lambda=10$, $\kappa=15.0$, and $d_P/H=0.05$ on (a) dimensionless temperature profiles using $\varepsilon=0.7$, (b) dimensionless temperature profiles using $\varepsilon=0.9$, and (c) total Nusselt number

**4.2 Variable Porosity.** For the variable porosity category, the reference value of dimensionless time $\tau$ is also based on the choice of intermediate values for the pertinent parameters. These reference values are 0.45 for the free stream porosity, 100 for the Reynolds number, and 0.05 for ratio of particle diameter to channel height. As mentioned earlier, permeability, Darcy number, the geometric function ($F$) and pressure gradient depend on the choice of the pertinent parameters for the variable porosity category. It is found that parameters (b) and (c) in Eq. (11) affect the velocity

profile but have insignificant effect on the location of the free surface front. Typical values for parameters (b) and (c) are assumed based on a previous study [5].

Results of the effect of the Reynolds number in Fig. 7 for the variable porosity category and for the constant porosity category given in Fig. 6 reveal that the general behavior of the relation between the free surface position and Reynolds number is not affected by introducing the effect of variable porosity. Particle diameter appears in the expressions for the variable porosity (Eq. 11) and the permeability expression (Eq. 12). It is found that
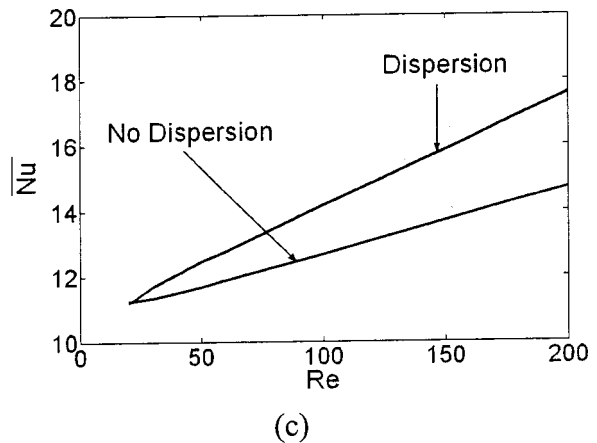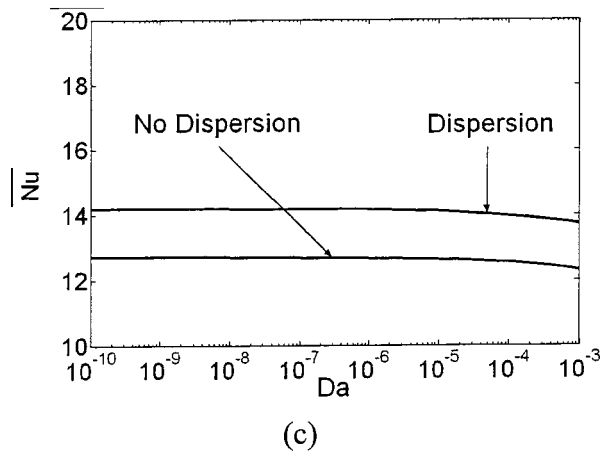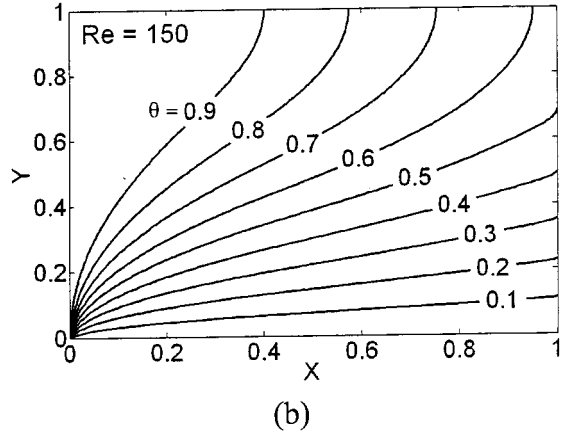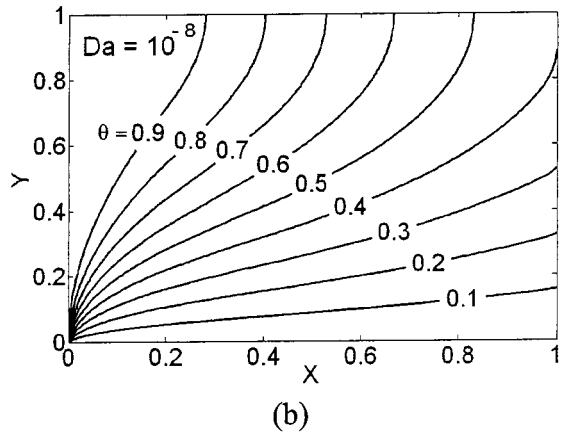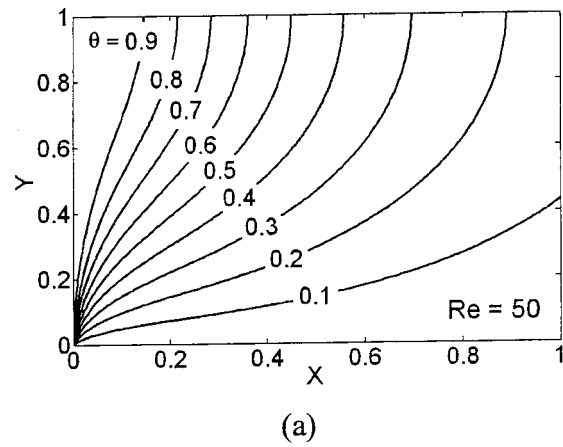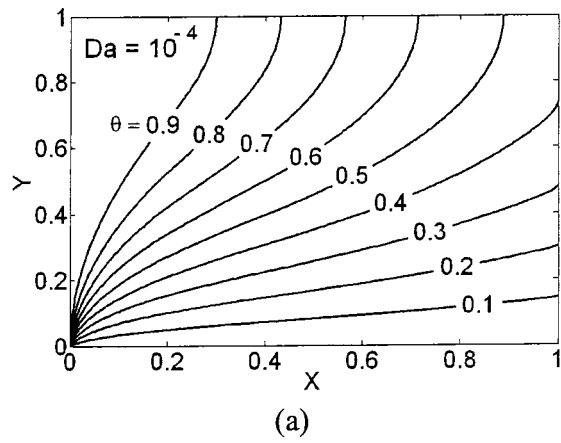
**Fig. 12 Effect of Darcy number for the thermal dispersion category using $\varepsilon=0.8$, Re=100, $\Lambda=10$, $\kappa=15.0$, and $d_P/H=0.05$ on (a) dimensionless temperature profiles using Da=$10^{-4}$, (b) dimensionless temperature profiles using Da=$10^{-8}$, and (c) total Nusselt number**

**Fig. 13 Effect of Reynolds number for the thermal dispersion category using $\varepsilon=0.8$ Da=$10^{-6}$, $\Lambda=10$, $\kappa=15.0$, and $d_P/H=0.05$ on (a) dimensionless temperature profiles using Re=50, (b) dimensionless temperature profiles using Re=150, and (c) total Nusselt number**

changing the particle diameter has an insignificant effect on the results. However, the influence of changing the particle diameter on the permeability is more significant. Particle diameter affects the value of Darcy number through the definition of permeability. Therefore, it is reasonable to compare the results of Fig. 8 for the particle diameter and the ones in Fig. 4 for the effects of variations in the Darcy number. The effect of Darcy number in Fig. 4 for the constant porosity category is more pronounced than the effect of variations in the particle diameter given in Fig. 8 for the variable porosity category.

**4.3 Thermal Dispersion.** The effect of thermal dispersion on the thermal characteristics of the free surface are analyzed in this section. Thermal equilibrium between the two phases is assumed. Introducing the effect of thermal dispersion in the energy equation in general favors conduction over convection. In other words, supplementing dispersion effects to the energy equation gives thermal conduction more dominance. This can be seen by comparing the temporal dimensionless temperature profiles in Figs. 9 and 10. Figure 9 illustrates the development of the temperature field with time with thermal dispersion effects included
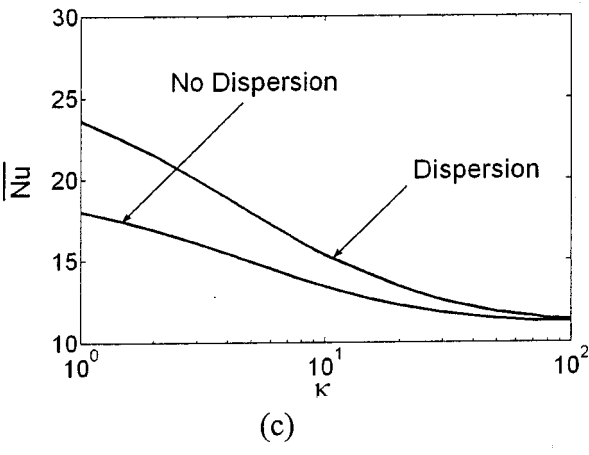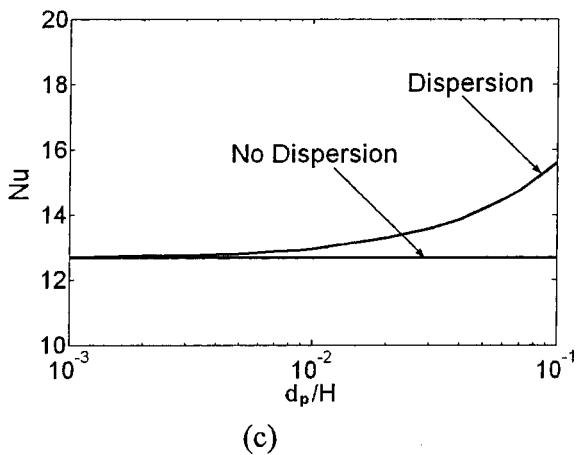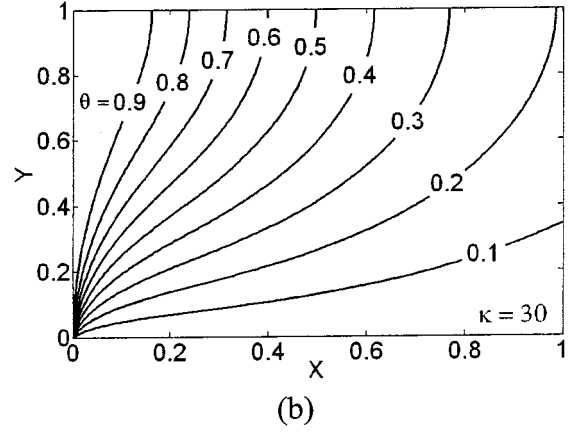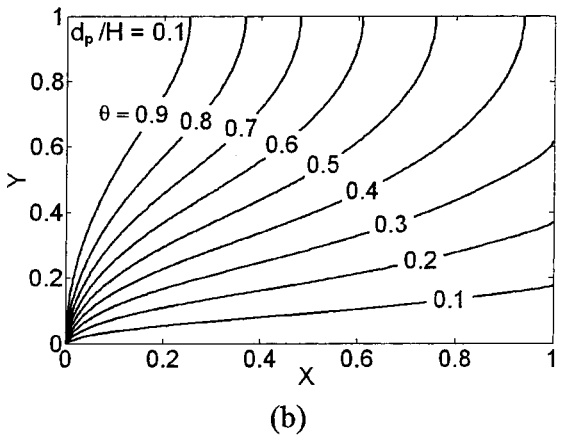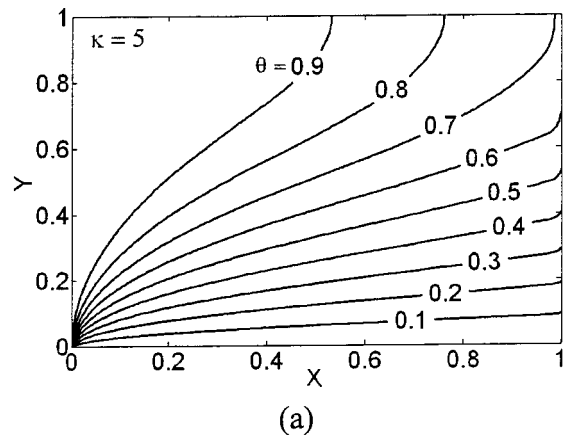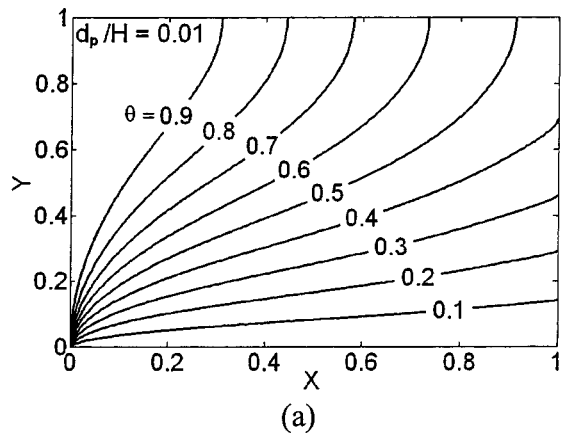
Fig. 14 Effect of particle diameter for the thermal dispersion category using $\varepsilon$=0.8 Da=$10^{-6}$, Re=100, $\Lambda$=10, and $\kappa$=15.0 on (a) dimensionless temperature profiles using $d_p$/H=0.01, (b) dimensionless temperature profiles using $d_P$/$H$=0.1, and (c) total Nusselt number



Fig. 15 Effect of solid-to-fluid thermal conductivity ratio, $\kappa$, for the thermal dispersion category using $\varepsilon$=0.8 Da=$10^{-6}$, Re =100, $\Lambda$=10, and $d_P$/$H$=0.05 on (a) dimensionless temperature profiles using $\kappa$=5.0, (b) dimensionless temperature profiles using $\kappa$=30.0, and (c) total Nusselt number

while Fig. 10 shows the same with thermal dispersion effects excluded while all other input parameters are kept the same. It is found that the total time taken to reach the end of the channel is the same for both cases.

Temperature contours and average Nusselt number curves for different values of porosity are shown in Fig. 11. It can be seen that higher porosity allows further thermal penetration of the encroaching fluid into the channel. Also, higher porosities result in higher Nusselt numbers as shown in Fig. 11(c). In addition, the difference between the two Nusselt numbers (with and without

dispersion) widens as porosity increases. Therefore, effect of thermal dispersion becomes more pronounced at higher porosities.

Temperature contours for relatively small and larger Darcy numbers are quite similar as seen in Figs. 12(a) and 12(b). Overall heat transfer characteristics are almost unaffected. The two Nusselt numbers, with and without the effect of dispersion, are almost the same for different Darcy numbers as shown in Fig. 12(c). However, both curves show a slight decrease as Da increases while keeping the same difference. Therefore, effect of Darcy number with the presence of thermal dispersion is relatively in-

(a)



(b)
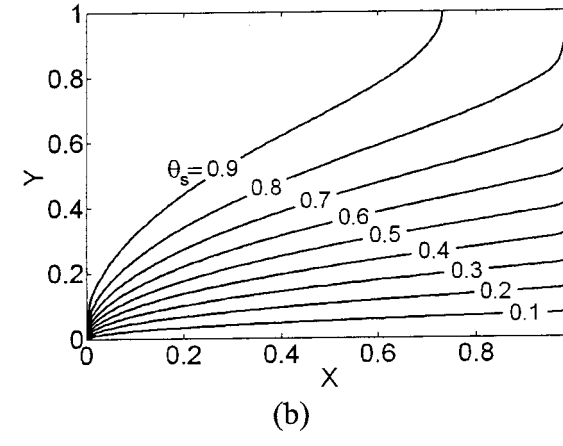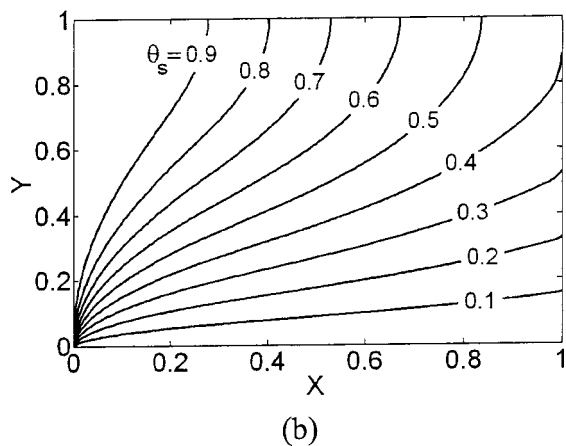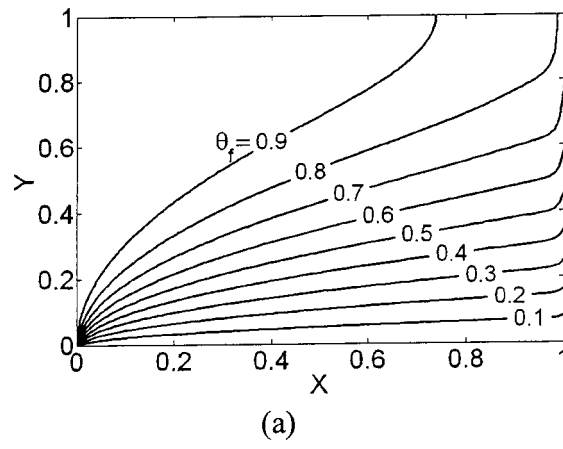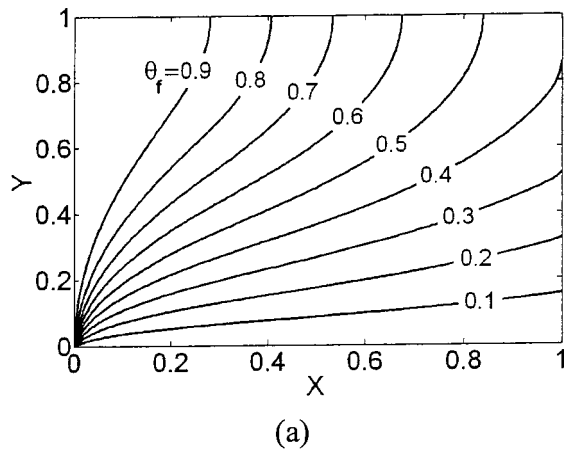
**Fig. 16 Dimensionless temperature profiles for the LTNE category using $\varepsilon$=0.8, Da=$10^{-6}$, Re=100, $\Lambda$=10, $\kappa$=15.0, and $d_P/H$=0.05: (a) fluid phase; and (b) solid phase**



(a)



(b)

**Fig. 17 Dimensionless temperature profiles for the LTNE category using $\varepsilon$=0.9, Da=$10^{-8}$, Re=200, $\Lambda$=100, $\kappa$=5.0, and $d_P/H$=0.1: (a) fluid phase; and (b) solid phase**

significant. Inertial parameter variation were also found to have an insignificant effect on the temperature distributions.

Effect of Reynolds number with the presence of thermal dispersion on temperature contours is shown in Figs. 13(a) and 13(b). As expected, heat transfer by convection is more dominant at higher Reynolds numbers. Reynolds number influence, with and without the presence of thermal dispersion, on the Nusselt number is depicted in Fig. 13(c). As can be seen the effect of thermal dispersion is relatively insignificant at very small Reynolds numbers. However, as Reynolds number increases, the effect of thermal dispersion becomes more pronounced. Figure 14 reveals that it is only important to account for the thermal dispersion effects for larger values of $d_p$.

Figures 15(a) and 15(b) present effect of solid-to-fluid conductivity ratio on temperature profiles when thermal dispersion effect is included. As can be seen in Fig. 15 temperature contours undergo a drastic change as this ratio changes. In Fig. 15(a) where a relatively smaller conductivity ratio is considered, the convective mode is more dominant since the effective conductivity is relatively smaller. As can be seen in Fig. 15(c), neglecting the thermal dispersion effect is a reasonable assumption only for relatively high conductivity ratios.

**4.4 Local Thermal Nonequilibrium.** In previous sections, local thermal equilibrium (LTE) between the solid and fluid phases was assumed. Figure 16 displays dimensionless temperature contours, under LTNE conditions while accounting for thermal dispersion. It is noted that temperatures of both phases are almost indistinguishable when moderate pertinent input param-

eters are used. When limiting input parameters are used as in Fig. 17, temperature difference between the two phases becomes more pronounced.

Effect of porosity variations on the average Nusselt numbers on LTNE is shown in Fig. 18. Figure 18(a) shows this effect while neglecting thermal dispersion. As can be seen the relatively small difference between the two Nusselt numbers remains constant as porosity changes. This is not the case when thermal dispersion effect is accounted for as demonstrated in Fig. 18(b). It is worth noting that the solid phase Nusselt number is almost the same with and without the effect of thermal dispersion.

Figure 19 shows the effect of Darcy number on the LTNE. For higher Darcy numbers, the two phases tend to reach thermal equilibrium as their Nusselt numbers intersect. Involvement of thermal dispersion enhances the effect of LTNE between the two phases as shown in Fig. 19(b). The inertia parameter effect is not significant on the Nusselt numbers as shown in Fig. 20, however, thermal dispersion widens the difference between the two Nusselt numbers as the inertia parameter changes. Once again, the solid phase Nusselt numbers are almost the same regardless of the presence or absence of thermal dispersion effects.

Increasing the Reynolds number increases the LTNE between the two phases with and without the effect of thermal dispersion. The involvement of thermal dispersion increases the sensitivity of LTNE to Reynolds number. The relation between the Nusselt numbers and Reynolds number remains linear for all cases even with the assumption of LTE as in Fig. 13. Particle diameter variations with and without the presence of thermal dispersion do not affect significantly the solid phase Nusselt numbers. However,

(a)



(b)
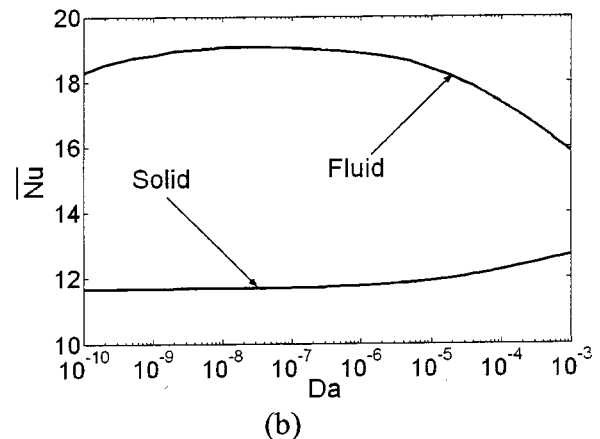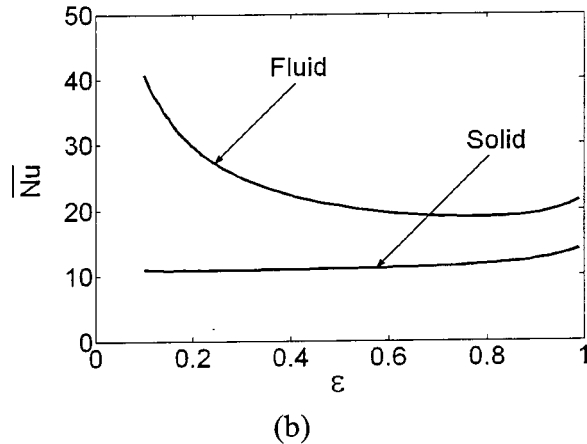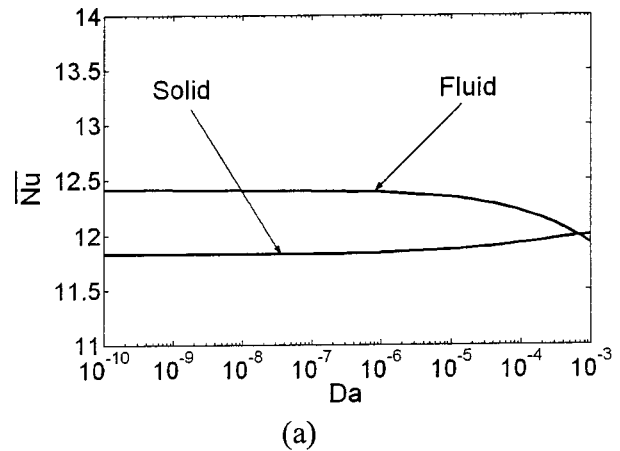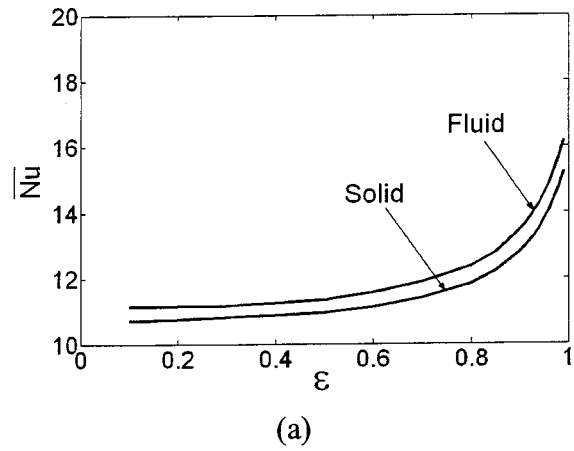
**Fig. 18  Effect of porosity on average Nusselt numbers for the LTNE category, Da=$10^{-6}$, Re=100, $\Lambda$=10, $\kappa$=15.0, and $d_P/H$ =0.05: (a) excluding thermal dispersion effects; and (b) including thermal dispersion effects**



(a)



(b)

**Fig. 19  Effect of Darcy number on average Nusselt numbers for the LTNE category, $\varepsilon$=0.8, Re=100, $\Lambda$=10, $\kappa$=15.0, and $d_P/H$=0.05: (a) excluding thermal dispersion effects; and (b) including thermal dispersion effects**

fluid phase Nusselt numbers increase as the value of particle diameter increases. Again, including thermal dispersion effects increases the response of the fluid phase Nusselt number to the changes in the particle diameter.

When thermal dispersion is not included, higher solid-fluid conductivity ratios cause a slight increase in the difference between the two Nusselt numbers. On the other hand, the difference between the two Nusselt numbers is almost constant when thermal dispersion effect is considered. It is worth noting that all Nusselt numbers decrease as the solid-to-fluid conductivity ratio increases for the same reasons discussed in the previous section.

## 5  Conclusions

A comprehensive analysis of variable porosity, thermal dispersion and local thermal nonequilibrium on free surface transport through porous media is presented in this study. Effects of pertinent parameters such as porosity of the porous medium, Darcy number, Inertia parameter, Reynolds number, particle diameter and solid-to-fluid conductivity ratio, on the momentum and thermal transport are analyzed and discussed. It is found that variable porosity effects can be quite substantial in the neighborhood of the solid boundaries. It is also shown that the thermal dispersion has a substantial effect on the thermal transport process. LTNE between the two phases is found to be more pronounced when thermal dispersion effect is included. Changes in porosity, Darcy number, Reynolds number and particle diameter on free surface transport are characterized and quantified. Therefore, ignoring these effects can lead to inaccurate estimations of the free surface problem.

## Nomenclature

$a_{sf}$ = specific surface area of the packed bed, $[\mathrm{m}^{-1}]$
$b, c$ = porosity variation parameters, Eq. (11)
$c_p$ = specific heat at constant pressure, $[\mathrm{J\,kg}^{-1}\mathrm{K}^{-1}]$
$d_p$ = particle diameter $[\mathrm{m}]$
Da = Darcy number, $K/H^2$
$F$ = geometric function defined in Eq. (13)
$h_{sf}$ = fluid-to-solid heat transfer coefficient, $[\mathrm{W\,m}^{-2}\mathrm{K}^{-1}]$
$H$ = half the height of the channel, $[\mathrm{m}]$
$J$ = unit vector aligned along the pore velocity
$k$ = thermal conductivity, $[\mathrm{W\,m}^{-1}\mathrm{K}^{-1}]$
$K$ = permeability $[\mathrm{m}^2]$
$L$ = length of the channel, $[\mathrm{m}]$
Nu = local Nusselt number
$\overline{\mathrm{Nu}}$ = average Nusselt number
$P$ = pressure, $[\mathrm{N/m}^2]$
Pr = Prandtl number, $\mu\,c_{Pf}/k_f$
Re = Reynolds number, $u_\infty H/\nu_f$
$\mathrm{Re}_K$ = particle Reynolds number, $u_c K^{1/2}/\nu$
$T$ = temperature, $[\mathrm{K}]$
$u$ = velocity in $x$-direction, $[\mathrm{m\,s}^{-1}]$
$x_0$ = free surface front location, $[\mathrm{m}]$
$x, y$ = Cartesian coordinates, $[\mathrm{m}]$
$X, Y$ = non-dimensional coordinates, $x/H$ and $y/H$
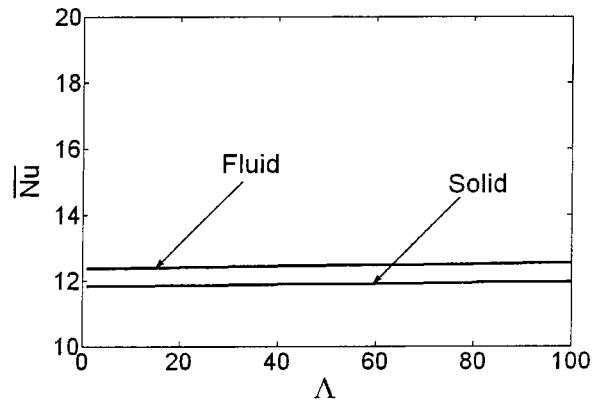
**(a)**
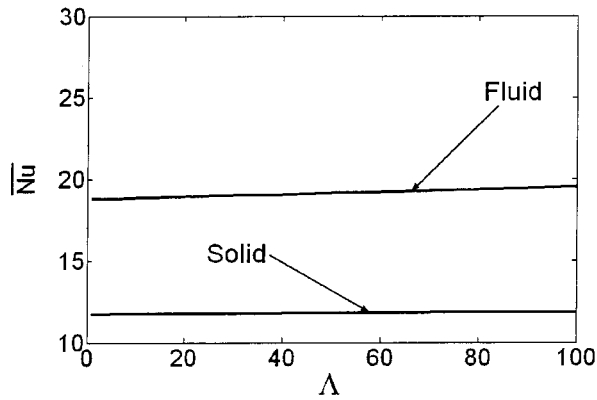


**(b)**

**Fig. 20  Effect of Inertia parameter on average Nusselt numbers for the LTNE category, $\varepsilon=0.8$, $Da=10^{-6}$, $Re=100$, $\kappa=15.0$, and $d_p/H=0.05$: (a) excluding thermal dispersion effects; and (b) including thermal dispersion effects**

**Greek Symbols**

$\alpha$ = thermal diffusivity, $[\text{m}^2\,\text{s}^{-1}]$
$\varepsilon$ = porosity
$\gamma$ = parameter
$\kappa$ = solid-to-fluid thermal conductivity ratio, $k_s/k_f$
$\Lambda$ = Inertia parameter, $\varepsilon^{3/2}Fu_\infty H/\nu_f$
$\mu$ = kinematics Viscosity, $[\text{kg}\,\text{m}^{-1}\text{s}^{-1}]$
$\nu$ = dynamic viscosity, $[\text{m}^2\,\text{s}^{-1}]$
$\theta$ = dimensionless temperature, $[(T_w-T)/(T_w-T_e)]$
$\rho$ = density, $[\text{kg}\,\text{m}^{-3}]$
$\tau$ = dimensionless time, Eq. (22)

**Subscripts**

$c$ = convective component
$e$ = inlet
$eff$ = effective property
$f$ = fluid
$m$ = mean
$max$ = maximum
$s$ = solid
$w$ = wall
$\infty$ = free stream

**Other Symbols**

$\langle\ \rangle$ = "local volume average" of a quantity

## References

[1] Muskat, M., 1937, *The Flow of Homogeneous Fluids Through Porous Media*, Edwards, Ann Arbor, MI.
[2] Srinivasan, V., and Vafai, K., 1994, "Analysis of Linear Encroachment in Two-Immiscible Fluid Systems in a Porous Medium," ASME J. Fluids Eng., **116**, pp. 135–139.
[3] Chen, S. C., and Vafai, K., 1996, "Analysis of Free Surface Momentum and Energy Transport in Porous Media," Numer. Heat Transfer, Part A, **29**, pp. 281–296.
[4] Chen, S. C., and Vafai, K., 1997, "Non-Darcian Surface Tension Effects on Free Surface Transport in Porous Media," Numer. Heat Transfer, Part A, **31**, pp. 235–254.
[5] Vafai, K., 1984, "Convective Flow and Heat Transfer in Variable-Porosity Media," J. Fluid Mech., **147**, pp. 233–259.
[6] Vafai, K., 1986, "Analysis of the Channeling Effect in Variable Porosity Media," ASME J. Energy Resour. Technol., **108**, pp. 131–139.
[7] Vafai, K., Alkire, R. L., and Tien, C. L., 1985, "An Experimental Investigation of Heat Transfer in Variable Porosity Media," ASME J. Heat Transfer, **107**, pp. 642–647.
[8] Amiri, A., and Vafai, K., 1994, "Analysis of Dispersion Effects and Non-Thermal Equilibrium, Non-Darcian, Variable Porosity, Incompressible Flow Through Porous Media," Int. J. Heat Mass Transfer, **37**, pp. 939–954.
[9] Hwang, G. J., Wu, C. C., and Chao, C. H., 1995, "Investigation of Non-Darcian Forced Convection in an Asymmetrically Heated Sintered Porous Channel," ASME J. Heat Transfer, **117**, pp. 725–732.
[10] Lee, D. Y., and Vafai, K., 1999, "Analytical Characterization and Conceptual Assessment of Solid and Fluid Temperature Differentials in Porous Media," Int. J. Heat Mass Transfer, **42**, pp. 423–435.
[11] Quintard, M., and Whitaker, S., 1995, "Local Thermal Equilibrium for Transient Heat Conduction: Theory and Comparison With Numerical Experiments," Int. J. Heat Mass Transfer, **38**, pp. 2779–2796.
[12] Quintard, M., Kaviany, M., and Whitaker, S., 1997, "Two-Medium Treatment of Heat Transfer in Porous Media: Numerical Results for Effective Properties," Adv. Water Resour., **20**, pp. 77–94.
[13] Quintard, M., and Whitaker, S., 1995, "The Mass Flux Boundary Condition at a Moving Fluid-Fluid Interface," Ind. Eng. Chem. Res., **34**, pp. 3508–3513.
[14] Quintard, M., and Whitaker, S., 1999, "Dissolution of an Immobile Phase During Flow in Porous Media," Ind. Eng. Chem. Res., **38**, pp. 833–844.
[15] Vafai, K., and Tien, C. L., 1981, "Boundary and Inertia Effects on Flow and Heat Transfer in Porous Media," Int. J. Heat Mass Transfer, **24**, pp. 195–203.
[16] Vafai, K., and Kim, S. J., 1989, "Forced Convection in a Channel Filled With a Porous Medium: An Exact Solution," ASME J. Heat Transfer, **111**, pp. 1103–1106.
[17] Sharif, N. H., and Wiberg, N. E., 2002, "Adaptive ICT Procedure for Non-Linear Seepage Flows With Free Surface in Porous Media," Commun. Numer. Methods Eng., **18**, pp. 161–176.
[18] Vafai, K., and Alazmi, B., 2003, "On the Line Encroachment in Two-Immiscible Fluid Systems in a Porous Medium," ASME J. Fluids Eng., **125**, pp. 738–739.